Signal processing for sidelobe suppression in optical coherence tomography images

Yingli Wang, Yanmei Liang,* and Kuanhong Xu

Institute of Modern Optics, Nankai University, Key Laboratory of Opto-electronic Information Science and Technology, Education Ministry of China, Tianjin 300071, China
**Corresponding author: ymliang@nankai.edu.cn*

Received July 24, 2009; revised December 10, 2009; accepted December 17, 2009;
posted December 17, 2009 (Doc. ID 114756); published February 11, 2010

In an optical coherence tomography system, the sidelobes of the point-spread function (PSF) introduced from the optical source reduce the A-scan imaging resolution and contrast of the images. A gradual iterative signal subtraction method based on the study of a point signal influenced by other points with different distances through the PSF is proposed in this paper. Comparing with the CLEAN algorithm and two typical deconvolution methods, the processed results demonstrate this algorithm can reduce sidelobes effectively with the least runtime. It is also found that it is insensitive to noise while slightly improving the longitudinal resolution, which shows this algorithm is good for improving image quality. © 2010 Optical Society of America

OCIS codes: 110.4500, 070.2025, 070.6110.

1. INTRODUCTION

Optical coherence tomography (OCT) is a relatively novel biomedical imaging technique that allows non-invasive and high-resolution imaging of biological tissue *in vivo* by using a low-temporal-coherence Michelson interferometer [1]. In an OCT system, the temporal coherence property of the light source or power spectrum governs the longitudinal point-spread function (PSF) of the imaging system, and thus the longitudinal resolution. Therefore, when the spectrum is non-Gaussian or not smooth, the point response in the interferogram will have sidelobes that can cause degradation of effective resolution and introduce artifacts that will lead to spurious structures in the OCT image.

Many efforts have been made toward sidelobe suppression in OCT by using different methods, including some hardware and software techniques. One hardware approach proposed in 2003 is using a programmable spectral processor to shape the power spectrum of the light source [2]. The software methods include the CLEAN algorithm of an iterative point-deconvolution algorithm [3,4], and some digital deconvolution methods that digitally modify the spectrum to make it more Gaussian [5–7]. However, if these software methods are not performed carefully, the noise of the resulting image can be greatly increased, which will cause degradation of image quality. The method of using a space-invariant linear post processing digital filter in which a sidelobe reduction filter is applied to the modulated signal to reduce sidelobes in the reconstructed image can minimize the increase in image noise [8].

By studying a point signal influenced by other points with different distances through the PSF, an algorithm of gradual iterative subtraction (GIS) is proposed to suppress sidelobes in this paper. The envelope of the signal is demodulated by digital filtering prior to the application of the algorithm. It is shown from the processing time that the algorithm is more efficient than deconvolution methods, which makes it attractive for use in real-time OCT imaging.

2. THEORY

The interferometric signal intensity for an OCT system based on a Michelson interferometer can be expressed as [9]

$$I(\tau) = 2\,\mathrm{Re}\{\langle \Gamma(\tau) * f(\tau)\rangle\}, \tag{1}$$

where τ is the time delay, the symbol $*$ denotes convolution, $f(\tau)$ is the impulse response function of the sample, and $\Gamma(\tau)$ is the coherence function of the light source, which is the inverse Fourier transform of the power spectral density (PSD) and is also regarded as the longitudinal PSF of the OCT system.

According to Eq. (1), for every point in an A-line of the OCT image, the measured signal in the spatial domain can be given as

$$g(x) = h(x) * f(x), \tag{2}$$

where $h(x)$ and $f(x)$ are the PSF of the OCT system and the sample pulse response signal, respectively. Ideally, according to Eqs. (1) and (2), the envelope signal of an isolated point is the convolution of the PSF and the sample pulse signal. Therefore, if the PSF has sidelobes, the degraded signal will be shown in the OCT image. Some deconvolution methods, such as the van Cittert method [10] and the Lucy–Richardson algorithm [11], can be used for signal restoring. However, for high-scattering specimens, such as biological tissues, the isolated points are nearly non-existent, so the convolution results of different scatters cannot be separated distinctly. These signals will be superimposed when coinciding in the spatial domain, which will obviously affect the deconvolution results. Therefore, in this case, any deconvolution methods will

have some limitation in eliminating the effect of the sidelobes. In addition, the noise that exists randomly in the system makes the problem more complicated.

In order to obtain a desirable result, a simple approach, performed for every A-line to obtain a sidelobe-reduced OCT image, is subtracting the sidelobes from the noisy signals directly. It is assumed that the signal of every point produces sidelobes, and the signal of every point is superimposed by the sidelobes of other points in the same A-line. According to Eq. (2), the degraded value of the point x_i in the spatial domain can be expressed as

$$g(x_i) = f(x_i) + \sum_{\substack{k=1 \\ (k \neq i)}}^{N} h(x_i - x_k) f(x_k), \tag{3}$$

where $f(x_i)$ and $g(x_i)$ are the original value and the degraded value of the point x_i, respectively. $f(x_k)$ is the original value of another point x_k. $h(x_i - x_k)$ is the value of the PSF at the point x_i when the PSF is centered at the point x_k. N is the number of the discrete points of the demodulated signal in the A-line, which is equal to the number of rows of the OCT image.

Thus, the influence on a point by the sidelobes of another point depends on the PSF of the OCT system and the spatial distance between them. Then, the original signal can be obtained by eliminating the influence of the sidelobes from other points, which can be expressed as

$$f(x_i) = g(x_i) - \sum_{\substack{k=1 \\ (k \neq i)}}^{N} h(x_i - x_k) f(x_k). \tag{4}$$

However, in practical OCT systems, all signals obtained are degraded, so $f(x_k)$ cannot be directly acquired and accurately calculated in accordance with Eq. (4). A simple iterative subtraction is introduced to approximate to Eq. (4):

$$f_j(x) = \begin{cases} f_{j-1}(x) - h(x - x_j) f_{j-1}(x_j), & x \neq x_j \\ f_{j-1}(x), & x = x_j \end{cases}, \tag{5}$$

where j is the number of iterations, the total iterations is N, $f_{j-1}(x_j)$ is the $(j-1)^{\text{th}}$ iterative result for the point x_j, and $f_0(x)$ is equal to $g(x)$.

The total processing steps in an A-line are given as follows. As a matter of convenience, the function $SL(x) = h(x - x_j) f_{j-1}(x_j)$ is defined:

(1) Measure the PSD of the light source at the sample arm of the OCT system.

(2) Calculate the normalized and discrete longitudinal PSF of the OCT system based on the measured PSD.The X-coordinate sampling interval of the PSF is the same as that of the demodulated signal. The X-coordinate range of the PSF is twice the scanning depth.

(3) Start from the first point x_1 of the degraded signal in an A-line, and translate the discrete PSF in the longitudinal direction to locate its maximum at the point x_1. The signal value of point x_1 is multiplied by the discrete PSF to obtain the function $SL(x)$.

(4) Subtract $SL(x)$ from the values of the other points, except the value of the point x_1.

(5) Translate the discrete PSF in the forward direction or from top to bottom, and calculate all points in the A-line as in steps (3) and (4) to obtain the first corrected result $f_{N\_1}(x)$.

(6) Start from the last point x_N in the same A-line, repeat steps (3) and (4), translate the discrete PSF in the reverse direction or from bottom to top, calculate all points in the same A-line again, and obtain the second corrected result $f_{N\_2}(x)$.

(7) Select the smaller of the corresponding points between the two corrected results as the final corrected result $f(x)$.

The segment flowchart of the algorithm in the forward direction is shown in Fig. 1.

3. RESULTS

To demonstrate the feasibility of the GIS algorithm for sidelobe suppression, the OCT signals of a few samples obtained from a time domain OCT system are processed. A typical fiber OCT system based on a Michelson interferometer is used, and a superfluorescent fiber light source that produces a broad but non-Gaussian spectrum is employed. The light source has a central wavelength around 1550 nm and an effective bandwidth of ~60 nm.

The optical interference signals from the sample arm and the reference arm are gathered by a balanced optical detector (New Focus 2117-FC) with a bandpass filter that transforms optical signals into electronic signals and minimizes the background optical noise by differential amplifying. The electronic signals, or interference signals modulated by the longitudinal PSF, are proportional to the incident light intensities. The electronic analog signals are directly collected by a DAQ (data acquisition) card with 2 MHz maximum sampling frequency to convert to digital signals.

The spatial period of the interference signals is $\lambda_0/2$, where λ_0 is the central wavelength of the light source. In terms of Nyquist sampling theorem and time efficiency, the detected analog signal for an A-line is digitized into 5000 data points by the DAQ card. The depth imaging range is 1.5 mm, so the spatial sampling period is 0.3 μm. The envelope of the A-line interference signal is demodulated by digital filtering and downconverted every 33 or 34 points into 150 peak data points in the this filtering process. The demodulated A-line signal consisting of these 150 data points is the linear OCT signal that will be the input of the algorithm. Every data point in the linear OCT signal corresponds to 10 μm in depth.

The PSD is measured by an optical spectrum analyzer, and the PSF is the inverse Fourier transform (FT) of the PSD. The PSD and PSF of the system [12] are shown in Fig. 2(a) and Fig. 2(b), respectively. The longitudinal range of the PSF used in the method is from −1.5 mm to 1.5 mm, and in order to show the PSF clearly, the range of X-coordinate in Fig. 2(b) is from −200 μm to 200 μm. To match the above sampling results, the quantification interval of the PSF in the iteration calculation is also adopted as 10 μm.

An air–mirror interface is used to determine the feasibility of sidelobe suppression for a single reflection. The

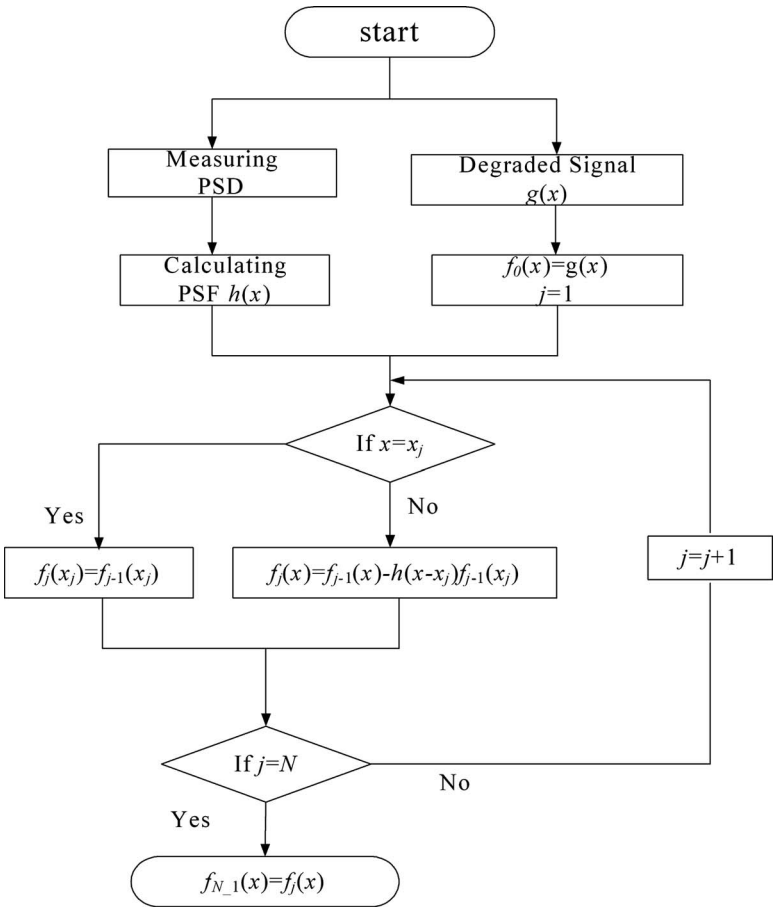

Fig. 1. Flowchart of the GIS algorithm in the forward direction in an A-line.

degraded image, the deconvolved images using the Lucy–Richardson algorithm and van Cittert's method, and the images corrected by the CLEAN algorithm and the GIS algorithm are shown in Figs. 3(a)–3(e), respectively. It must be stated, the signals are processed in linear scale in all of the algorithms. The images are used only to show the final processing results. When the signals are converted into images, the maximum signal is taken as gray value 255 in the image. Signal processing is performed with a PC equipped with an Intel Core 2 Processor (1.86 GHz main frequency), and the algorithms are written with a home-developed MATLAB-based software. The runtimes of the Lucy–Richardson algorithm, van Cittert's method, the CLEAN algorithm, and the GIS algorithm for 200 A-scans are about 0.9 s, 7 s, 0.6 s and 0.4 s, respectively.

It can be seen from Figs. 3(c)–3(e) that sidelobes in the processed images are reduced. It is also shown in Fig. 3(b) that the Lucy–Richardson algorithm can make the interface clearer, but it has no significant effect on sidelobe reduction. The van Cittert method can obviously suppress sidelobes, but its processing time is so long that it is not fit for real-time processing. Figures 3(a)–3(e) are shown directly with the linear signals. They are enhanced by his-

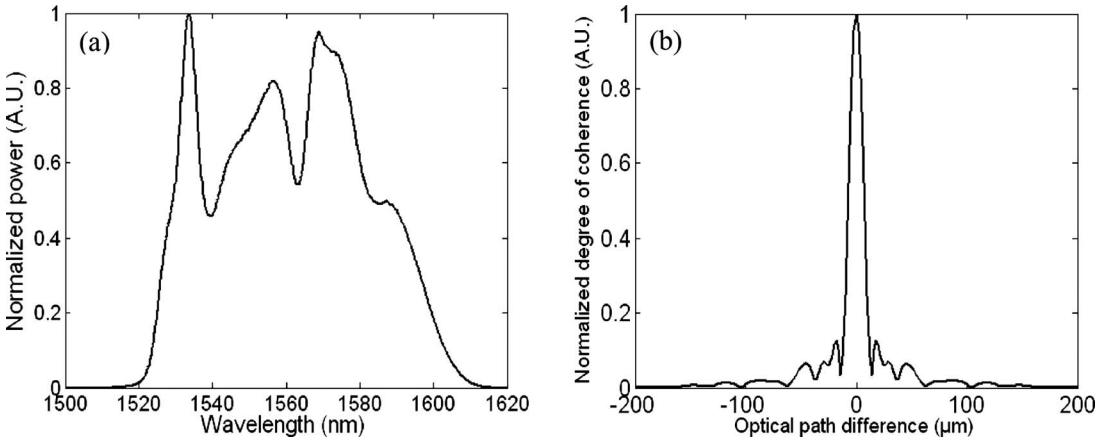

Fig. 2. (a) Measured PSD and (b) the normalized corresponding coherence function of the light source.

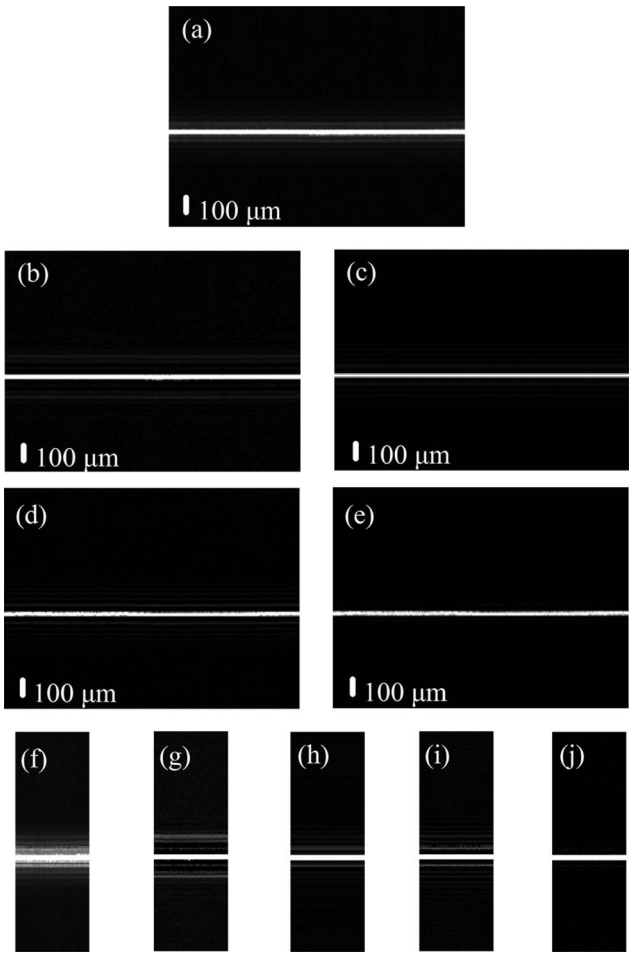

Fig. 3. OCT images of the air–mirror interface: (a) degraded image, (b) deconvolved image by Lucy–Richardson algorithm, (c) deconvolved image by van Cittert's method, (d) corrected image by the CLEAN algorithm, (e) corrected image by the GIS algorithm. (f)—(j) are the extracted parts from the enhanced images of (a)—(e), respectively: (f) degraded image, (g) deconvolved image by Lucy–Richardson algorithm, (h) deconvolved image by van Cittert's method, (i) corrected image by the CLEAN algorithm, (j) corrected image by the GIS algorithm.

togram equalization to make the difference clearer in visual effect, whose subregions are shown in Figs. 3(f)–3(j), respectively. An arbitrary A-scan result in Figs. 3(a), 3(d), and 3(e) is shown in Fig. 4 to reveal the sidelobe suppression quantitatively. Compared with −20 dB (the anterior sidelobe) and −23 dB (the posterior sidelobe) reductions by the CLEAN algorithm shown by a blue dotted curve—the degraded signal of −16.6 dB is shown as a red dashed curve—the sidelobes are reduced to −28.6 dB and −45 dB by using the GIS algorithm, shown by a green solid curve, respectively.

The second example image is of the pulp of an orange with the same OCT system. The degraded image is shown in Fig. 5(a), and the images corrected by the CLEAN algorithm and the GIS algorithm are shown in Figs. 5(b) and 5(c), respectively. Enlarged images of the rectangular boxes in Figs. 5(a)–5(c) are shown in Figs. 5(d)–5(f) for closely displaying the performance of the algorithms. It is shown that the contrast between the air and the pulp surface has been improved, and the internal structure of the pulp is delineated well. An arbitrary A-scan signal of Fig. 5 is shown in Fig. 6. The sidelobe in the front surface of the pulp is reduced from −15 dB to −16.4 dB (suppressed by the CLEAN algorithm) and −30.4 dB (by the GIS algorithm), which demonstrates that coherent artifacts can be significantly removed.

A degraded OCT image of the index finger is shown in Fig. 7(a), and the images corrected by the CLEAN algorithm and the GIS algorithm are shown in Figs. 7(b) and 7(c), respectively. Enlarged images of the rectangular boxes in Figs. 7(a)–7(c) are shown in Figs. 7(d)–7(f). The sidelobes in Fig. 7(c) are reduced much more than those in Fig. 7(b). An arbitrary A-scan signal of Fig. 7 is shown in Fig. 8. The sidelobe in the front surface of the index figure is reduced from −14.5 dB to −16.8 dB (suppressed by the CLEAN algorithm) and −23.3 dB (by the GIS algorithm).

As the orange and index finger are high-scattering specimens, the intensities of the light scattered from the interior of them are much lower than those from the surface. All the images in Fig. 5 and Fig. 7 are obtained by using the exponential transform [13] from linear signals to improve the visual effect for the interior structure.

In order to evaluate the influence of the algorithms on

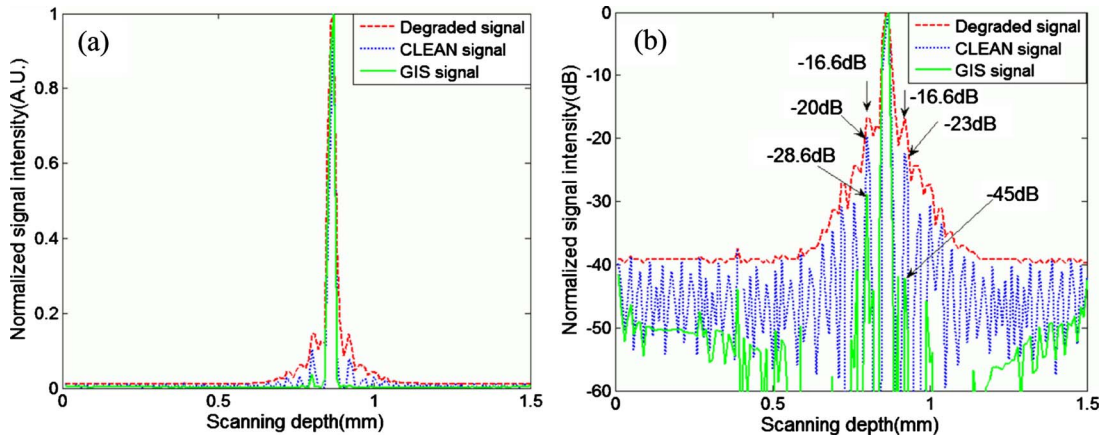

Fig. 4. (Color online) Normalized signals of an arbitrary A-scan line of the air–mirror interface in Fig. 3: (a) linear signals, (b) logarithmic signals. The degraded signal, the signal corrected by the CLEAN algorithm, and the signal corrected by the GIS algorithm are shown by red dashed, blue dotted, and green solid curves, respectively.

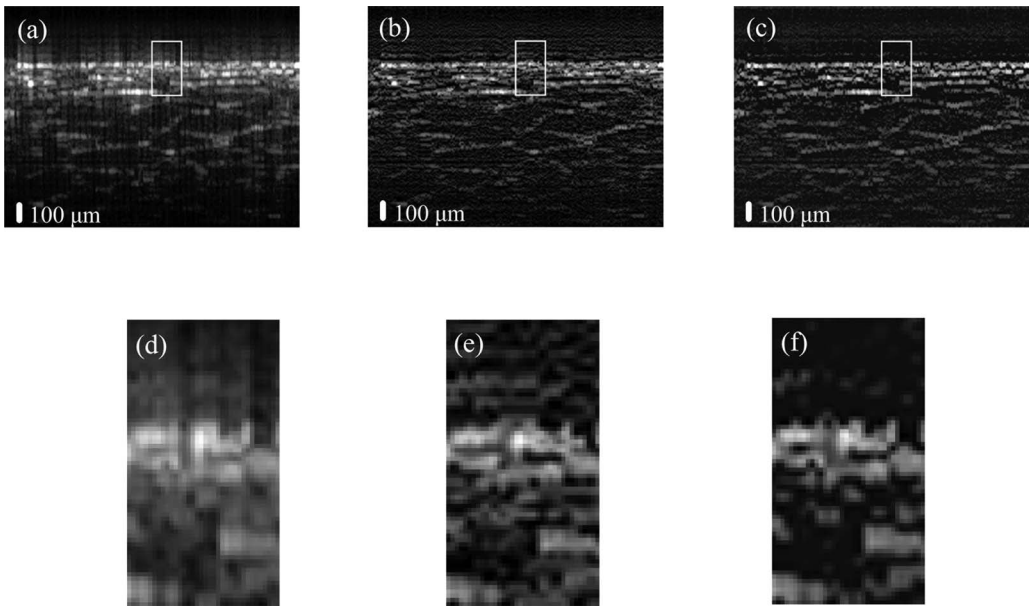

Fig. 5. OCT images of orange pulp: (a) degraded image, (b) corrected image by the CLEAN algorithm, (c) corrected image by the GIS algorithm. Three enlarged images in the rectangular boxes of (a)—(c) are shown in (d)—(f): (d) degraded image, (e) corrected image by the CLEAN algorithm, and (f) corrected image by the GIS algorithm.

the image quality, the signal-to-noise ratio (*SNR*) is calculated. The formula for the *SNR* can be expressed as [14]

$$SNR = 10 \log_{10}[\max(X_s)^2/\sigma_n^2]. \quad (6)$$

As the GIS algorithm is based on signal processing in the longitudinal direction, unlike the definition of [14], the above formula represents the *SNR* of a certain column in the image. $\max(X_s)$ and σ_n represent the maximum signal and the background noise variance in the column on the linear intensity scale, respectively. Then, the *SNR*s of all columns in the image are averaged to obtain the average *SNR* of the image. The average *SNR*s of Figs. 3(a), 3(d), and 3(e) are 50.23 dB, 48.34 dB, and 55.85 dB, those of Figs. 5(a)–5(c) are 36.54 dB, 34.85 dB, and 38.02 dB, and those of Figs. 7(a)–7(c) are 37.31 dB, 36.41 dB, and 39.57 dB, respectively. The average *SNR*s in Figs. 3(e), 5(c), and 7(c) are increased by 5.62 dB, 1.48 dB, and 2.26 dB over those of the degraded images, respectively, which means that the GIS algorithm can improve the image quality to some degree. It is also shown that the average *SNR*s of the CLEAN algorithm become slightly lower than those of other deconvolution methods [3].

4. DISCUSSIONS

From the above results, we can see that sidelobe reduction in a single reflection interface can reach up to 28.4 dB by the GIS algorithm. The respective sidelobe reductions of 15.4 dB and 8.8 dB in the images of the orange pulp and the index finger demonstrate the efficacy of the GIS algorithm in turbid biological samples. Although the brightness of the corrected image is slightly decreased, some image enhancement methods can be used to enhance the visual effect. It is also shown in Fig. 4 and Fig. 6 that longitudinal resolution is slightly improved.

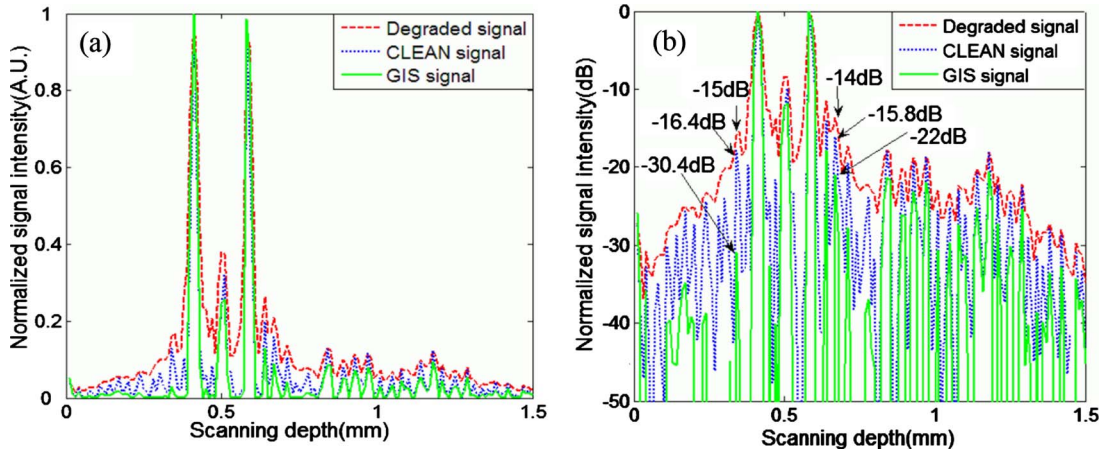

Fig. 6. (Color online) Normalized signal intensity of an arbitrary A-scan line of the orange pulp in Fig. 5: (a) linear signals, (b) logarithmic signals. The degraded signal, the signal corrected by the CLEAN algorithm, and the signal corrected by the GIS algorithm are shown by red dashed, blue dotted, and green solid curves, respectively.

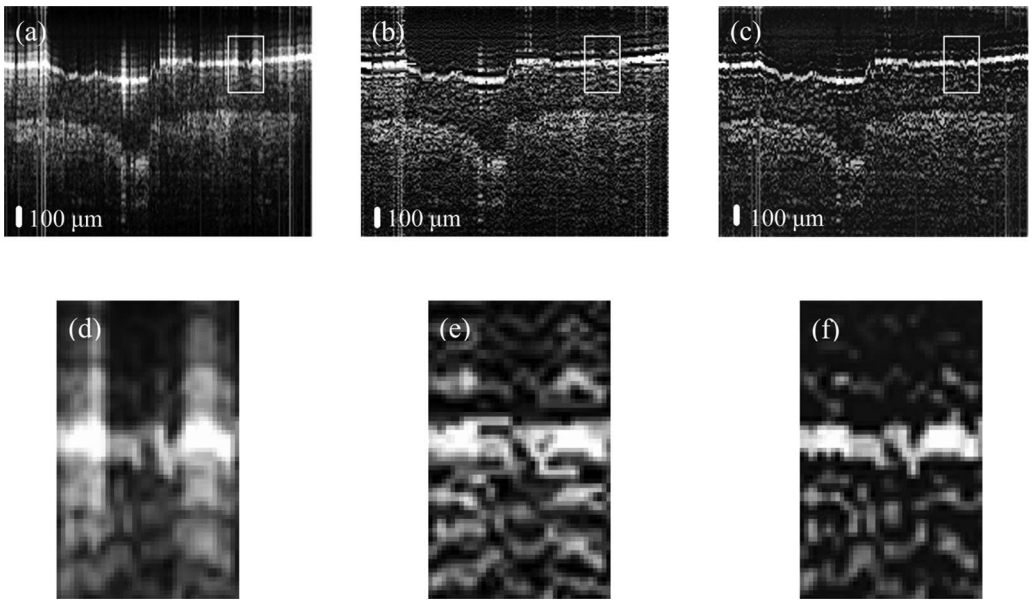

Fig. 7. OCT images of the index finger: (a) degraded image, (b) corrected image by the CLEAN algorithm, (c) corrected image by the GIS algorithm. Three enlarged images in the rectangular boxes of (a)—(c) are shown in (d)—(f): (d) degraded image, (e) corrected image by the CLEAN algorithm, (f) corrected image by the GIS algorithm.

The method involves the PSF of the system, so the PSD of the light source is measured from the sample arm, not directly from the exit of the light source. This can avoid the possible distortion of the PSD when light is transmitted in the fiber, although it is not observed in our OCT system. In addition, the dispersion between the two arms must be balanced. An all-reflective optical delay line [15] is used in the experiments to avoid introducing excess dispersion.

Figures 9(a) and 9(b) are linear signals of an arbitrary A-scan of the air–mirror interface obtained with the GIS algorithm by iterating in the forward and reverse direction, respectively. It is shown in Fig. 9 that the degree of sidelobe suppression is related to the processing direction (indicated by a horizontal arrow). The sidelobe suppression of the posterior points (relative to the processing direction) is less effective than that of the anterior points. The reason is that the value of $f_{j-1}(x_j)$ of Eq. (5) is closer to the original value with the increase of j in the iteration processing. This leads to the sidelobes due to the posterior points being more accurate, so that the anterior points degraded by the sidelobes of the posterior points will be closer in value to the original signals after correction. The minimum value of the two iterations in the forward and reverse directions is chosen as the final corrected value in this paper.

Although the GIS algorithm does not specifically consider the effect of the noise in the iteration process, it is of interest to note that the average *SNR* is increased. The denoising mechanism will be the focus of further research. In addition, as the algorithm is based on the PSF of the OCT system and the sampling data, it may fail to achieve desirable results when the uniformity of the peak-value interval during digital filtering is compromised. More refined quantification may be the answer to this.

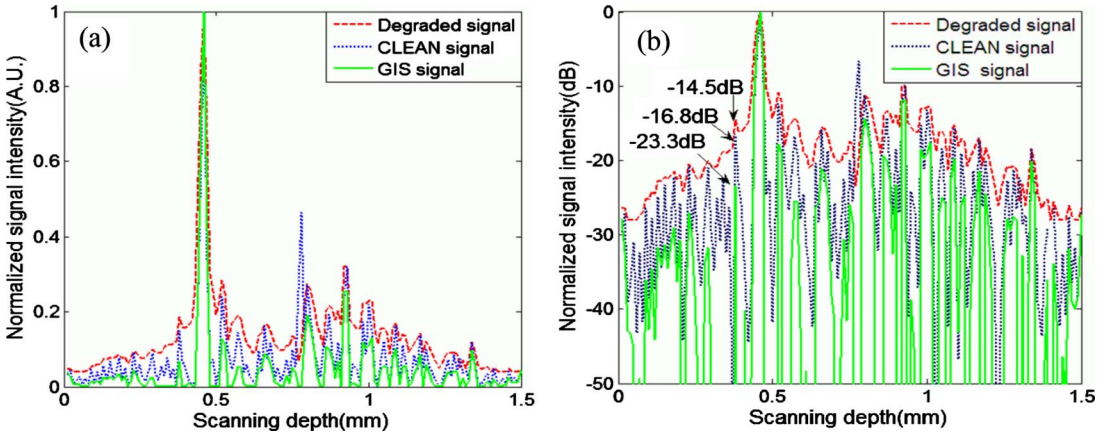

Fig. 8. (Color online) Normalized signal intensity of an arbitrary A-scan line of the index finger in Fig. 7: (a) linear signals, (b) logarithmic signals. The degraded signal, the signal corrected by the CLEAN algorithm, and the signal corrected by the GIS algorithm are shown by red dashed, blue dotted, and green solid curves, respectively.

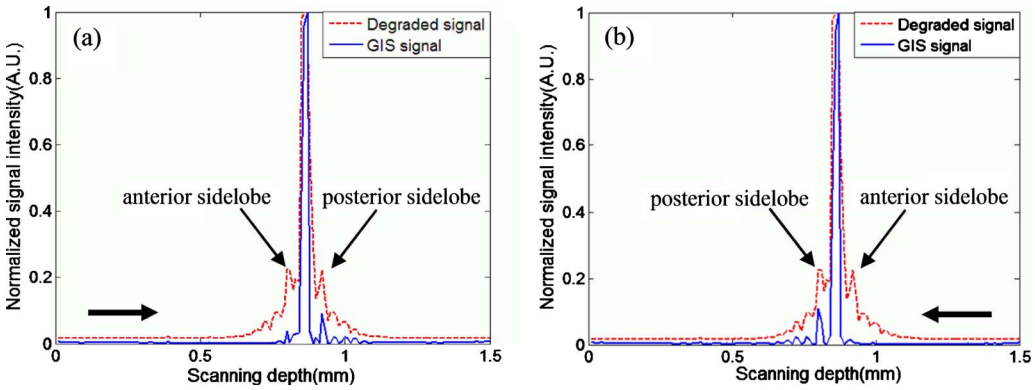

Fig. 9. (Color online) Normalized linear signals of an arbitrary A-scan line of the air–mirror interface: (a) degraded signal and corrected signal obtained by the iterative processing in the forward direction, (b) degraded signal and corrected signal obtained by the iterative processing in the reverse direction. Degraded signal and corrected signal are shown by red dashed and blue solid curves, respectively. Horizontal arrow indicates the processing direction.

5. CONCLUSION

Sidelobes may introduce deceptive information into a real OCT signal that degrades the image. In order to suppress sidelobes, the method of gradual iterative subtraction is proposed, and its effectiveness is proved with the result of the air–mirror interface OCT image. The corrected OCT images of the orange tissue and the index finger show its efficacy in turbid biological samples. The method in this paper provides a more robust means of obtaining the original data from the degraded. In addition, it enhances the quality of the image significantly and makes the internal microstructure easier to distinguish. Its higher efficiency shows that the GIS algorithm has strong potential for real-time processing.

ACKNOWLEDGMENTS

This research is supported by the National Natural Science Foundation of China (NSFC) (Grant Nos. 60637020 and 60677012) and the Tianjin Foundation of Natural Science (No. 09JCZDJC18300).

REFERENCES

1. D. Huang, E. A. Swanson, C. P. Lin, J. S. Schuman, W. G. Stinson, W. Chang, M. R. Hee, T. Tlotte, K. Gregory, C. A. Puliafito, and J. G. Fujimoto, "Optical coherence tomography," Science **254**, 1178–1181 (1991).
2. A. C. Akcay and J. P. Rolland, "Spectral shaping to improve the point spread function in optical coherence tomography," Opt. Lett. **28**, 1921–1923 (2003).
3. J. M. Schmitt, "Restoration of optical coherence images of living tissue using the CLEAN algorithm," J. Biomed. Opt. **3**, 66–75 (1998).
4. D. Piao, Q. Zhu, N. K. Dutta, S. Yan, and L. L. Otis, "Cancellation of coherent artifacts in optical coherence tomography imaging," Appl. Opt. **40**, 5124–5131 (2001).
5. R. Tripathi, N. Nassif, J. S. Nelson, B. H. Park, and J. F. de Boer, "Spectral shaping for non-Gaussian source spectra in optical coherence tomography," Opt. Lett. **27**, 406–408 (2002).
6. J. F. de Boer, C. E. Saxer, and J. S. Nelson, "Stable carrier generation and phase-resolved digital data processing in optical coherence tomography," Appl. Opt. **40**, 5787–5790 (2001).
7. E. D. J. Smith, S. C. Moore, N. Wada, W. Chujo, and D. D. Sampson, "Spectral domain interferometry for OCDR using non-Gaussian broad-band sources," IEEE Photonics Technol. Lett. **13**, 64–66 (2001).
8. D. Marks, P. S. Carney, and S. A. Boppart, "Adaptive spectral apodization for sidelobe reduction in optical coherence tomography images," J. Biomed. Opt. **9**, 1281–1287 (2004).
9. A. F. Fercher, W. Drexler, C. K. Hitzenberger, and T. Lasser, "Optical coherence tomography—principles and applications," Rep. Prog. Phys. **66**, 239–303 (2003).
10. G. Thomas, "An improvement of the van-Cittert's method," in *Proceedings of IEEE International Conference on Acoustics Speech, Speech, and Signal Processing* (IEEE, 1981), pp. 47–49.
11. R. C. Gonzalez and R. E. Woods, *Digital Image Processing* (Prentice Hall, 2002).
12. Y. Liu, Y. Liang, G. Mu, and X. Zhu, "Deconvolution methods for image deblurring in optical coherence tomography," J. Opt. Soc. Am. A **26**, 72–77 (2009).
13. Y. Liu, Y. Liang, Z. Tong, X. Zhu, and G. Mu, "Contrast enhancement of optical coherence tomography images using least squares fitting and histogram matching," Opt. Commun. **279**, 23–26 (2007).
14. D. C. Adler, T. H. Ko, and J. G. Fujimoto, "Speckle reduction in optical coherence tomography images by use of a spatially adaptive wavelet filter," Opt. Lett. **29**, 2878–2880 (2004).
15. X. Liu, M. J. Cobb, and X. Li, "Rapid scanning all-reflective optical delay line," Opt. Lett. **29**, 80–82 (2004).